PCCP

Accepted Manuscript

ROYAL SOCIETY OF CHEMISTRY

www.rsc.org/pccp

Unravelling Optical Responses of Nanoplasmonic Mirror-on-Mirror Metamaterials

Debabrata Sikdar[*, a], Shakeeb B. Hasan[b], Michael Urbakh[c], Joshua B. Edel[a], and Alexei A. Kornyshev[*, a]

[a] *Department of Chemistry, Faculty of Natural Sciences, Imperial College London, Exhibition Road, South Kensington, London, SW7 2AZ, United Kingdom*

[b] *Complex Photonic Systems (COPS), MESA+ Institute for Nanotechnology, University of Twente, PO Box 217, 7500 AE Enschede, The Netherlands*

[c] *School of Chemistry, University of Tel-Aviv, Ramat-Aviv, Israel*

Corresponding e-mails: [*]d.sikdar@imperial.ac.uk, [*]a.kornyshev@imperial.ac.uk

Keywords: plasmonics, nanoparticles, optical metamaterials, metallic films, mirror-on-mirror, reflectivity

Mirror-on-mirror platforms based on arrays of metallic nanoparticles, arranged top-down or self-assembled on a thin metallic film, have interesting optical properties. Interaction of localized surface-plasmons in nanoparticles with propagating surface-plasmons in the film underpins exotic features of such platforms. Here, we present a comprehensive theoretical framework which emulates such system using a five-layer-stack model and calculate its reflectance, transmittance, and absorbance spectra. The theory rests on dipolar quasi-static approximations incorporating image-forces and effective medium theory. Systematically tested against full-wave simulations, this simple approach proves to be adequate within its obvious applicability limits. It is used to study optical signals as a function of nanoparticle dimensions, interparticle separation, metal film thickness, gap between the film and nanoparticles, and incident light characteristics. Several peculiar features are found, such as, e.g. quenching reflectivity in certain frequency domains, or shift of the reflectivity spectra. Schemes are proposed to tailor those as functions of the mentioned parameters. Calculating the system's optical responses in seconds, as compared to much longer running simulations, this theory helps to momentarily unravel the role of each system parameter on light reflection, transmission, and absorption, facilitating thereby design and optimisation of novel mirror-on-mirror systems.

Introduction

The coherent oscillation of conduction electrons in metallic **n**ano**p**articles (NPs) gives rise to the phenomenon called localized surface plasmon resonance (LSPR), which has enabled numerous exotic features in the optical responses of various plasmonic NP based systems[1–7]. These NPs facilitate intense confinement of near-field in sub-wavelength volumes, surpassing the traditional diffraction limit of light[8,9]. This not only permits localization and transportation of energy down to nanoscale, but also exhibits strikingly new far-field features such as directed narrowband-scattering and resonance-enhanced wide-band absorption of light for different applications[3–7,10–13]. The spectral position, width, and intensity of the LSPR can be tuned as functions of size, shape, composition, and surrounding medium of individual NPs[14–18]. When these free-standing NPs are arranged to form a linear chain or a two-dimensional (2D) periodic array, their collective LSPR properties depend also on inter-particle spacing, lattice orientation, as well as light polarization and the angle of incidence. [19–23]). For NPs on a metallic substrate, image interactions further affects LSPR as function of the structure of the NP array, the material of the substrate, as well as the separation between NPs and the substrate[10,24–27].

Amongst various metamaterials[28–30] mirror-on-mirror structures are of particular interest because of their tailorable and potentially tuneable optical properties[31–33]. In such systems, a 2D array of metallic NPs is assembled on top of a metallic film, in most cases, with a thin dielectric spacer in between. This gives rise to intense coupling between the LSPR of the NPs with the propagating plasmons on the thin metallic film[34,35]. The optical responses of these film-coupled NPs are found to be highly sensitive to any changes in the gap between NPs or their distance from the film. With the virtue of sensitive gap-dependent plasmonic responses, these mirror-on-mirror assemblies are deployed mostly in sensing applications[35–38], but they may be equally interesting for developing novel optical devices[3,9,39–41], which could produce tuneable reflection or transmission of light or amplify its harvesting.

Assembly or stimulated self-assembly of NPs at interfaces of two different media have been studied for quite a while[42–47]. But precise fabrication and accurate experimental characterization of such systems remain a hot topic of research in a number of several groups[42–44], including our's[46,48,49]. Though there are a few reports on how to theoretically investigate the optical responses of NPs at an interface consisting semi-infinite dielectric or metallic substrate [48–50], studies on mirror-on-mirror comprising NPs on thin metallic films are thus far conducted only based on experiments and numerical simulations. In this paper we bridge the gap and present the first *comprehensive* theory for estimating the optical response spectra of a realistic metal-on-metal assembly by considering NP

array coupled to a metallic film of finite thickness. Here we abstract ourselves from how the arrays self-assemble and build the structures of interest, but will present a detailed analysis of optical response of NP arrays in such systems.

There are two methods of exciting plasmonic effects in such mirror-on-mirror assemblies. One is to follow white light dark-field illumination scheme, where light is impinging from the top *i.e.*, directly on the NPs[35,38]. This method excites LSPR of the NPs, which then radiates into far-field as well as into a non-resonant continuum of propagating plasmon modes on the surface of the gold film[38]. The other method involves shining of light from the bottom, *i.e.*, directly on the metallic film through a scheme called white light total-internal-reflectance illumination[35,38]. This method can excite a single resonant propagating plasmon mode at a fixed angle of incidence, where phase-matching condition is met by that plasmonic mode[4,35,38]. This implies that coupling between NP plasmons and film plasmons would be more intense in the second case; however the setup needs to follow stringent requirement of phase-matching that restricts its wide and diverse applications. Therefore, here we focus only on the first case and present its theoretical formulation. A similar approach can be adopted for modelling of the system under the other illumination scheme and will be reported elsewhere.

The theory presented here is an extension of the modified effective medium theory[48,49,51,52] with several modifications, and which is now based on a five-layer stack that specifically incorporates thin metallic film. The theory itself is based on dipolar approximation of optical response of NPs, takes into account image dipoles emerging at the interface, all incorporated into a multi-reflection theory. Within defined and physically justified limits, thus calculated optical response spectra, agree exceptionally well with numerically computed ones based on full-wave simulations. The latter affirms accuracy and effectiveness of this simplistic theoretical framework in emulating complex mirror-on-mirror systems comprising film-coupled plasmonic NPs.

The theory can be used to describe the role of different system parameters and understand how the interplay between those could modify the system response, for the rational design of such architectures. Note that it takes just seconds on a personal computer to calculate one spectrum based on the theory, whereas simulations often take much longer. Thus, the theory could provide a perfect platform allowing 'feed-back mode' analysis to design and optimize different exciting optical features of mirror-on-mirror assemblies as novel optical metamaterials.

In the subsequent sections we provide complete derivation of this theory with explicit expressions to obtain reflectance, transmittance and absorbance spectra. In what follows is a detailed analysis of the exciting features of these optical responses as functions of 'lattice' spacing,

thickness of the dielectric spacer layer and of the thin metallic film, the size of NPs, and characteristics of the impinging light such as incident angle and polarization Peaks and dips in reflection spectra are found to be very sensitive to the system parameters. We physically explain each highlighted effect and different aspects of its tuneability, which is one of the goals of the paper. Those effects could enable new applications such as optical switching, variable reflectance mirrors, and ultra-sensitive detection, with their ability to provide dynamically tuneable responses by mere alteration of incident light characteristics.

Theoretical Framework

Figure 1 displays the idea of the reduction of the optical response of a nanoplasmonic mirror-on-mirror structure (Figure 1 (a)) to the one of a five-layer stack system quasi-static, Figure 1(b), using effective-medium theory. The previous versions of this theory, developed for the case of a semi-infinite metal substrate involved four layers have been reported in Refs.[46,48,49]. They comprised a development of few older works [51,52] on freestanding NP arrays to particularly account for contributions arising from the image dipoles. Here, we introduce an additional layer and re-derive all equations for the five-layer model simultaneously correcting some minor inconsistencies in the previous derivations with fewer layers in the stack. The new framework would allow us to readily calculate optical responses of nanoplasmonic mirror-on-mirror assemblies, which thus far have been commonly studied only using time-consuming numerical computations. The present article presents the devised theoretical framework in detail and systematically compares its results with the full-wave simulations.

In the system under study (Figure 1), light is considered to incident at an angle θ to the normal to the plane of NPs, while propagating with wavevector ***k*** in the layer 1 ('half-space'), which represents the dielectric medium of optical dielectric constant ε_1 surrounding the layer of NPs . We demonstrate that in order to emulate the optical response from an ordered array of metallic NPs, each of radius R, the NP monolayer in Figure 1(a) can be represented as a uniform layer (layer 2) in Figure 1 (b) with effective thickness d. Layer 2 can be characterized using an anisotropic frequency-dependent dielectric tensor with components $\varepsilon_2^{\parallel}(\omega)$ and $\varepsilon_2^{\perp}(\omega)$, derived and discussed in the subsequent paragraphs. The NPs are considered to be arranged in a two-dimensional (2D) hexagonal array with lattice constant a, and are positioned on a dielectric spacer (layer 3) of height h_s that separates the NP layer from the metallic film (layer 4) of thickness (or height) h_f. In practice, layer 3 could represent the layer of ligands protecting the metal surface; it could stand for a solid dielectric

spacer, if there is such, or even the embedding medium of the NPs if the NPs are attached to the surface by rare ligands; this layer can be attributed optical dielectric constant ε_3. Layer 2 could represents the layer of NPs, which themselves are functionalized (covered) by their own ligands immersed in the dielectric medium of the same optical dielectric constant ε_1 as the half-space 1. Generally $\varepsilon_1 \neq \varepsilon_3$, but for the sake of simplicity we will put theme equal to each other. Layer 4 depicts a metallic film and has a frequency-dependent dielectric response, expressed as $\varepsilon_4(\omega)$. Layer 5 ('half-space') represents the substrate material, typically glass or PET, on which the metallic film (layer 4) is placed. The optical properties of layer 5 is taken into calculations through a dielectric constant ε_5.

The material properties and physical parameters of such five-layer stack models could be chosen independently for designing any application-specific mirror-on-mirror system. Although to exemplify the results we will stick to certain choice of material parameters, but apart from simplification $\varepsilon_1 \neq \varepsilon_3$, all equations will be presented in the most general form.

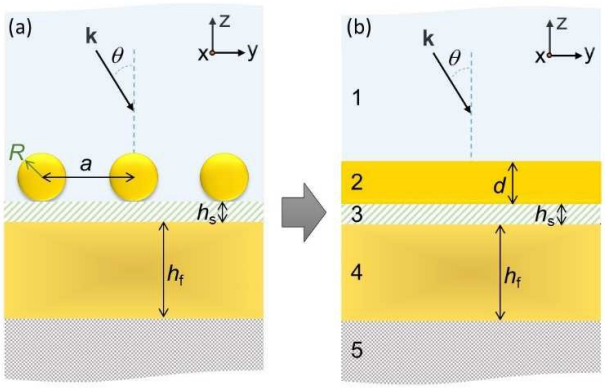

Figure 1. Theoretical model emulating a realistic nanoplasmonic mirror-on-mirror structure. Schematic representation of nanoparticles (NPs) in a dielectric medium forming a 2D array when placed on a metallic film with a spacer layer in between. A practical system (a) is emulated using a five-layer stack model (b) in order to estimate its optical responses. Incident light propagates in a semi-infinite medium, layer 1, with wavevector ***k*** and incident angle θ. Layer 2 of thickness d emulates an ordered array of metallic NPs, (each of radius R) with lattice constant a. The NPs are placed on a metallic film (layer 4 of height h_f) with a dielectric spacer layer (layer 3 of height h_s) in between. Layer 5 represents a semi-infinite dielectric medium on top of which the metallic film (layer 4) is placed.

The phenomena of reflection, transmission, and absorption of incident light comprise the far-field response of any optical system. Each of these contributing factors in a five-layer stack system can be calculated using reflection and transmission coefficients for homogeneous multi-layer stacks[53]. While implementing this strategy the most significant part is to accurately characterize the effective dielectric function of the metallic NP monolayer, which is represented as layer 2 in Figure 1(b). The dielectric response of a metal at optical wavelengths is strongly affected by the inter-band transitions. This demands the **D**rude (D) permittivity model for metal dielectric function to be extended to a **D**rude–**L**orentz (DL) model [46]:

$$\varepsilon_{\mathrm{DL}}(\omega) = \varepsilon_{\infty} - \frac{\omega_{\mathrm{p,D}}^2}{\omega^2 + i\gamma_{\mathrm{D}}\omega} - \frac{s_1\omega_{\mathrm{p1,L}}^2}{(\omega^2 - \omega_{\mathrm{p1,L}}^2) + i\gamma_{\mathrm{1,L}}\omega} - \frac{s_2\omega_{\mathrm{p2,L}}^2}{(\omega^2 - \omega_{\mathrm{p2,L}}^2) + i\gamma_{\mathrm{2,L}}\omega}. \quad (1)$$

Here ε_{∞} is the permittivity limit at high frequencies, which describes the polarizability due to valence electrons of the ionic skeleton of the metal, $\omega_{\mathrm{p,D}}$ and γ_{D} denote plasma frequency and damping coefficient from the Drude model, respectively. The third and the fourth terms in Eq. (1) are the two additional **L**orentzians (L) with resonance frequencies $\omega_{\mathrm{p1,L}}$ and $\omega_{\mathrm{p2,L}}$, with $\gamma_{\mathrm{1,L}}$ and $\gamma_{\mathrm{2,L}}$ representing the spectral widths of the two resonances where s_1 and s_2 are their weighting factors.

Note that the results of the theory presented below will be applied to the systems of gold NPs on a gold film. Whereas the latter is, from many points of view, one of the best substrates for mirror-on-mirror systems, one can certainly experiment with different kinds of NPs, including composite NPs[2,46,54]. However, without any loss of generality, we will restrict our attention to providing a proof-of-principle and not consider other possible cases which could be nonetheless interesting in a particular experimental realization of these systems. Thus here we will deal exclusively with the dielectric function of gold, for which the parameters of Eq. (1), best fitting the experimental data [55], are listed in Table1:

Table 1. Parameters of the Drude-Lorentz model for gold

ε_{∞}	$\omega_{\mathrm{p,D}}$ (eV)	γ_{D} (eV)	s_1	$\omega_{\mathrm{p1,L}}$ (eV)	$\gamma_{\mathrm{1,L}}$ (eV)	s_2	$\omega_{\mathrm{p2,L}}$ (eV)	$\gamma_{\mathrm{2,L}}$ (eV)
5.9752	8.8667	0.03799	1.76	3.6	1.3	0.952	2.8	0.737

For a monolayer of subwavelength spherical NPs of radius R ($<<\lambda$), forming an ordered hexagonal 2D array, the effective quasi-static polarizability of individual NPs can be expressed as

$$\beta_{\parallel}(\omega)=\frac{\alpha(\omega)}{1+\alpha(\omega)\frac{1}{\varepsilon_1}\left[\frac{-1}{2}\frac{U_A}{a^3}+\xi(\omega)\left(\frac{f(h,a)}{a^3}-\frac{3}{2}\frac{g_1(h,a)}{a^3}+\frac{1}{8h^3}\right)\right]} \quad (2a)$$

$$\beta_{\perp}(\omega)=\frac{\alpha(\omega)}{1+\alpha(\omega)\frac{1}{\varepsilon_1}\left[\frac{U_A}{a^3}-\xi(\omega)\left(\frac{f(h,a)}{a^3}-12\frac{h^2 g_2(h,a)}{a^5}-\frac{1}{4h^3}\right)\right]} \quad (2b)$$

Both Eqs. (2a) and (2b) have been corrected w.r.t. Eqs. (12) and (13) of Ref [48]. Namely, the expressions for the image contribution that stand in the parenthesis multiplying $\xi(\omega)$ had to be changed to correct the inconsistencies found in their previous versions. To be precise, in Eq. (2a) the second term in the image contributions for $\beta_{\parallel}(\omega)$ is corrected w.r.t. to similar term in equation (12) of Ref [48]. In equation(2b) the second and third terms in the image contributions for $\beta_{\perp}(\omega)$ have also been revised, replacing the similar terms in Eq. (13) of Ref [48]. The function $g_2(h,a)$ has been newly introduced in this process as part of the $\beta_{\perp}(\omega)$ expression. Note that in $\beta_{\parallel,\perp}(\omega)$ expressions, U_A sums up the contributions from all NPs in the monolayer interacting with any given NP, $f(h,a)$, $g_1(h,a)$ and $g_2(h,a)$ contribute towards adding up the effects arising from images of the all 'other' NPs, whereas the last term with $1/h^3$ dependency incorporates the effects from the NP's own image. The intensity of the obtained optical response can be related to $\left|\beta_{\parallel,\perp}(\omega)\right|$.

Here, $\alpha(\omega)$ represents the isotropic polarizability of each individual free-standing NP in the quasi-static dipolar approximation, given by

$$\alpha(\omega)=\varepsilon_1 R^3\frac{\varepsilon_{\mathrm{NP}}(\omega)-\varepsilon_1}{\varepsilon_{\mathrm{NP}}(\omega)+2\varepsilon_1}\ , \quad (3)$$

with ε_1 being the medium in which the NP with permittivity $\varepsilon_{\mathrm{NP}}(\omega)\equiv\varepsilon_{\mathrm{DL}}(\omega)$ is immersed. As explained above in the introduction of the model, we consider NPs arrays to be positioned on top of a metallic film with finite thickness, from which NPs are separated by a thin dielectric spacer layer of

dielectric constant ε_3, which as mentioned we will put $\varepsilon_3 = \varepsilon_1$. In this scenario, the image-charge screening factor of the metallic film can be expressed as

$$\xi(\omega) = \frac{\varepsilon_1 - \varepsilon_4(\omega)}{\varepsilon_1 + \varepsilon_4(\omega)} \ , \tag{4}$$

with $\varepsilon_4(\omega)$ being the permittivity of the metallic film. Considering in the paper gold films, we will put $\varepsilon_4(\omega) \equiv \varepsilon_{\mathrm{DL}}(\omega)$, but of course generally any other metals, e.g. silver, could be considered.

Note, such simplified account of image forces is equivalent to replacing the metal film by a semi-infinite metal slab. This is, however, justified if the layer of NPs is close to the boundary with the metal film. Then the effective dipoles representing NPs do not 'see' the glass (layer 5) behind the metallic film, *i.e.* the effect of its finite thickness becomes inconsequential. The exact criterion when such approximation is possible (on the thickness of the film, its dielectric constant, and the distance of dipoles from the film) can be obtained. But even without going into this rigorous analysis, a simple study by COMSOL Multiphysics® for the films of the thickness of studied in this article shows no difference from the case of semi-infinite film. Furthermore the form of expression for image terms neglects the possible difference between the values of the optical dielectric constants of the layers 1 and 3, which as we have already mentioned have been assumed, for simplicity, to be the same. Had we taken all those neglected differences, the equations would have become very cumbersome. At the same time there is not much need of it, because the difference between the expected values of these dielectric constants is very small. Furthermore, with some penetration of the solvent from region 1 to 3, the difference might practically vanish.

The lattice dependent parameter U_A and $f(h,a)$, $g_1(h,a)$ and $g_2(h,a)$ functions in Eq. (2) are calculated from the sums over the hexagonal lattice and are expressed as:

$$U_A = {\sum_i}' {\sum_j}' \frac{1}{\left(i^2 + j^2 - ij\right)^{3/2}} = 11.031, \qquad f(h,a) = {\sum_i}' {\sum_j}' \frac{1}{\left(i^2 + j^2 - ij + \left(\frac{2h}{a}\right)^2\right)^{3/2}},$$

$$g_1(h,a) = {\sum_i}' {\sum_j}' \frac{\left(i^2 + j^2\right)}{\left(i^2 + j^2 - ij + \left(\frac{2h}{a}\right)^2\right)^{5/2}}, \qquad g_2(h,a) = {\sum_i}' {\sum_j}' \frac{1}{\left(i^2 + j^2 - ij + \left(\frac{2h}{a}\right)^2\right)^{5/2}},$$

where $h = h_s + R$ is the height of the point dipoles from the surface of the metallic film. In case of a square lattice, these are of the following form:

$$U_A = \sum_i {}' \sum_j {}' \frac{1}{\left(i^2 + j^2\right)^{3/2}} = 9.031\,, \qquad f(h,a) = \sum_i {}' \sum_j {}' \frac{1}{\left(i^2 + j^2 + \left(\frac{2h}{a}\right)^2\right)^{3/2}},$$

$$g_1(h,a) = \sum_i {}' \sum_j {}' \frac{\left(i^2 + j^2\right)}{\left(i^2 + j^2 + \left(\frac{2h}{a}\right)^2\right)^{5/2}}, \qquad g_2(h,a) = \sum_i {}' \sum_j {}' \frac{1}{\left(i^2 + j^2 + \left(\frac{2h}{a}\right)^2\right)^{5/2}}$$

In a similar manner, any other lattice orientation of the NPs can be considered in our theoretical formulation. The changes in the model would be only in the terms of lattice sum parameter U_A and $f(h,a)$, $g_1(h,a)$ and $g_2(h,a)$ functions in Eq. (2), where one needs to express the distance of each lattice point from a reference point in terms of the primitive vectors of that particular lattice geometry.

Using the effective dipolar polarizabilities in Eq. (2), the effective dielectric permittivity $\varepsilon_2(\omega)$ of such an NP layer can be estimated as

$$\varepsilon_2^{\parallel}(\omega) = \varepsilon_1 + \frac{4\pi}{a^2 d}\beta_{\parallel}(\omega)\,, \tag{5a}$$

$$\frac{1}{\varepsilon_2^{\perp}(\omega)} = \frac{1}{\varepsilon_1} - \frac{1}{\varepsilon_1^2}\frac{4\pi}{a^2 d}\beta_{\perp}(\omega)\,, \tag{5b}$$

where $\varepsilon_2^{\parallel}(\omega)$ and $\varepsilon_2^{\perp}(\omega)$ are the components of the dielectric tensor parallel and perpendicular to the plane of the NP monolayer, a is the lattice constant in the array of NPs (centre-to-centre distance), and d is the characteristic thickness of the emulated NP monolayer (layer 2 in Figure 1(b)).

With the knowledge of dielectric permittivity of each layer, the next step is to connect the coefficients of reflection and transmission across all interfaces between the layers of the five-layer stack system. A transfer matrix $\widetilde{\mathrm{M}}_{\mathrm{n}}$ that relates the reflection (r) and transmission (t) coefficients from each interface n between layers n and $n+1$ is given by[53],

$$\widetilde{\mathrm{M}}_{\mathrm{n}} = \frac{1}{t_{n,n+1}}\begin{pmatrix} e^{-i\delta_{n+1}} & r_{n,n+1}e^{i\delta_{n+1}} \\ r_{n,n+1}e^{-i\delta_{n+1}} & e^{i\delta_n+1} \end{pmatrix}, \tag{6}$$

with $2\delta_{n+1}$ being the phase difference between the two reflected waves in layer n: one reflected straightaway from the interface between layer n and $n+1$; and another gets transmitted through that interface. The latter passes through layer $n+1$, gets reflected from the next interface and then

returns by passing through layer $n+1$ again to be finally transmitted into layer n. For a five-layer stack system (which has four interfaces) the total transfer matrix is given by $\widetilde{\mathrm{M}} = \widetilde{\mathrm{M}}_1 \cdot \widetilde{\mathrm{M}}_2 \cdot \widetilde{\mathrm{M}}_3 \cdot \widetilde{\mathrm{M}}_4$ i.e.:

$$\widetilde{\mathrm{M}} = \frac{1}{t_{1,2}}\begin{pmatrix} e^{-i\delta_2} & r_{1,2}e^{i\delta_2} \\ r_{1,2}e^{-i\delta_2} & e^{i\delta_2} \end{pmatrix} \cdot \frac{1}{t_{2,3}}\begin{pmatrix} e^{-i\delta_3} & r_{2,3}e^{i\delta_3} \\ r_{2,3}e^{-i\delta_3} & e^{i\delta_3} \end{pmatrix} \cdot \frac{1}{t_{3,4}}\begin{pmatrix} e^{-i\delta_4} & r_{3,4}e^{i\delta_4} \\ r_{3,4}e^{-i\delta_4} & e^{i\delta_4} \end{pmatrix} \cdot \frac{1}{t_{4,5}}\begin{pmatrix} 1 & r_{4,5} \\ r_{4,5} & 1 \end{pmatrix}. \tag{7}$$

The overall reflection coefficient from such system is then calculated as $\tilde{r} = \widetilde{\mathrm{M}}_{21} / \widetilde{\mathrm{M}}_{11}$, where $\widetilde{\mathrm{M}}_{21}$ and $\widetilde{\mathrm{M}}_{11}$ are the elements of the total transfer matrix of Eq. (7). Hence, $\tilde{r}$ can be expressed as

$$\tilde{r} = \frac{\begin{bmatrix} r_{12} + r_{12}r_{34}r_{45}e^{2i\delta_4} + r_{12}r_{23}r_{34}e^{2i\delta_3} + r_{12}r_{23}r_{45}e^{2i\delta_3}e^{2i\delta_4} + r_{23}e^{2i\delta_2} \\ +r_{23}r_{34}r_{45}e^{2i\delta_2}e^{2i\delta_4} + r_{34}e^{2i\delta_2}e^{2i\delta_3} + r_{45}e^{2i\delta_2}e^{2i\delta_3}e^{2i\delta_4} \end{bmatrix}}{\begin{bmatrix} 1 + r_{34}r_{45}e^{2i\delta_4} + r_{23}r_{34}e^{2i\delta_3} + r_{23}r_{45}e^{2i\delta_3}e^{2i\delta_4} + r_{12}r_{23}e^{2i\delta_2} \\ +r_{12}r_{23}r_{34}r_{45}e^{2i\delta_2}e^{2i\delta_4} + r_{12}r_{34}e^{2i\delta_2}e^{2i\delta_3} + r_{12}r_{45}e^{2i\delta_2}e^{2i\delta_3}e^{2i\delta_4} \end{bmatrix}}. \tag{8}$$

As the Fresnel coefficients are in general different for the s- and p-polarization of light, it is convenient to explicitly express the reflection coefficient as

$$\tilde{r}^{(\mathrm{s,p})} = \frac{\begin{bmatrix} r_{12}^{(\mathrm{s,p})} + r_{12}^{(\mathrm{s,p})}r_{34}^{(\mathrm{s,p})}r_{45}^{(\mathrm{s,p})}s_4 + r_{12}^{(\mathrm{s,p})}r_{23}^{(\mathrm{s,p})}r_{34}^{(\mathrm{s,p})}s_3 + r_{12}^{(\mathrm{s,p})}r_{23}^{(\mathrm{s,p})}r_{45}^{(\mathrm{s,p})}s_3s_4 + r_{23}^{(\mathrm{s,p})}s_2^{(\parallel,\perp)} \\ +r_{23}^{(\mathrm{s,p})}r_{34}^{(\mathrm{s,p})}r_{45}^{(\mathrm{s,p})}s_2^{(\parallel,\perp)}s_4 + r_{34}^{(\mathrm{s,p})}s_2^{(\parallel,\perp)}s_3 + r_{45}^{(\mathrm{s,p})}s_2^{(\parallel,\perp)}s_3s_4 \end{bmatrix}}{\begin{bmatrix} 1 + r_{34}^{(\mathrm{s,p})}r_{45}^{(\mathrm{s,p})}s_4 + r_{23}^{(\mathrm{s,p})}r_{34}^{(\mathrm{s,p})}s_3 + r_{23}^{(\mathrm{s,p})}r_{45}^{(\mathrm{s,p})}s_3s_4 + r_{12}^{(\mathrm{s,p})}r_{23}^{(\mathrm{s,p})}s_2^{(\parallel,\perp)} \\ +r_{12}^{(\mathrm{s,p})}r_{23}^{(\mathrm{s,p})}r_{34}^{(\mathrm{s,p})}r_{45}^{(\mathrm{s,p})}s_2^{(\parallel,\perp)}s_4 + r_{12}^{(\mathrm{s,p})}r_{34}^{(\mathrm{s,p})}s_2^{(\parallel,\perp)}s_3 + r_{12}^{(\mathrm{s,p})}r_{45}^{(\mathrm{s,p})}s_2^{(\parallel,\perp)}s_3s_4 \end{bmatrix}}. \tag{9}$$

Here $s_2^{(\parallel,\perp)} = e^{2ik_2^{(\parallel,\perp)}d}$, $s_3 = e^{2ik_3h_\mathrm{s}}$ and $s_4 = e^{2ik_4h_\mathrm{f}}$ are the phase factors; $k_2^{(\parallel,\perp)}$ are the parallel/perpendicular components of the wave vector in layer 2, k_3 and k_4 denote the wave vectors in layer 3 and 4 respectively; and r_{ij} are the reflection coefficients at the i/j interface given by

$$r_{ij}^{\mathrm{s}} = \frac{k_i^{\parallel}(\omega) - k_j^{\parallel}(\omega)}{k_i^{\parallel}(\omega) + k_j^{\parallel}(\omega)}, \tag{10a}$$

$$r_{ij}^{\mathrm{p}} = \frac{\varepsilon_i^{\parallel}(\omega)k_j^{\perp}(\omega) - \varepsilon_j^{\parallel}(\omega)k_i^{\perp}(\omega)}{\varepsilon_i^{\parallel}(\omega)k_j^{\perp}(\omega) + \varepsilon_j^{\parallel}(\omega)k_i^{\perp}(\omega)}. \tag{10b}$$

The wave vectors in Eq. (10) are given by:

$$k_1(\omega) = \frac{\omega}{c}\sqrt{\varepsilon_1}\cos\theta, \tag{11a}$$

$$k_2^{\parallel}(\omega)=\frac{\omega}{c}\sqrt{\varepsilon_2^{\parallel}(\omega)-\varepsilon_1\sin^2\theta}\,, \tag{11b}$$

$$k_2^{\perp}(\omega)=\frac{\omega}{c}\left(\frac{\varepsilon_2^{\parallel}(\omega)}{\varepsilon_2^{\perp}(\omega)}\right)^{1/2}\sqrt{\varepsilon_2^{\perp}(\omega)-\varepsilon_1\sin^2\theta}\,, \tag{11c}$$

$$k_3(\omega)=\frac{\omega}{c}\sqrt{\varepsilon_3(\omega)-\varepsilon_1\sin^2\theta}\,, \tag{11d}$$

$$k_4(\omega)=\frac{\omega}{c}\sqrt{\varepsilon_4(\omega)-\varepsilon_1\sin^2\theta}\,, \tag{11e}$$

$$k_5(\omega)=\frac{\omega}{c}\sqrt{\varepsilon_5(\omega)-\varepsilon_1\sin^2\theta}\,, \tag{11f}$$

where $\varepsilon_2^{(\parallel,\perp)}(\omega)$ are the parallel and perpendicular components of the dielectric constant of layer 2, and $\varepsilon_i^{\parallel}(\omega)=\varepsilon_i^{\perp}(\omega)=\varepsilon_i\,(\omega)$ for $i=1,\ 3$, 4 and 5.

This theoretical framework allows one to calculate reflectance $R^{(\mathrm{s,p})}$ from the five-layer stack system as of $R^{(\mathrm{s,p})}=\left|\tilde{r}^{(\mathrm{s,p})}\right|^2$. In a similar manner the transmittance $T^{(\mathrm{s,p})}$ through this system can be expressed as $T^{(\mathrm{s,p})}=\left|\tilde{t}^{(\mathrm{s,p})}\right|^2$, where $\tilde{t}^{(\mathrm{s,p})}\equiv\frac{1}{\tilde{\mathrm{M}}_{11}}$ is given by:

$$\tilde{t}^{(\mathrm{s,p})}=\frac{t_{12}^{(\mathrm{s,p})}t_{23}^{(\mathrm{s,p})}t_{34}^{(\mathrm{s,p})}t_{45}^{(\mathrm{s,p})}s_2^{(\parallel,\perp)}s_3s_4}{\left[\begin{array}{c}1+r_{34}^{(\mathrm{s,p})}r_{45}^{(\mathrm{s,p})}s_4+r_{23}^{(\mathrm{s,p})}r_{34}^{(\mathrm{s,p})}s_3+r_{23}^{(\mathrm{s,p})}r_{45}^{(\mathrm{s,p})}s_3s_4+r_{12}^{(\mathrm{s,p})}r_{23}^{(\mathrm{s,p})}s_2^{(\parallel,\perp)}+r_{12}^{(\mathrm{s,p})}r_{23}^{(\mathrm{s,p})}r_{34}^{(\mathrm{s,p})}r_{45}^{(\mathrm{s,p})}s_2^{(\parallel,\perp)}s_4\\ +r_{12}^{(\mathrm{s,p})}r_{34}^{(\mathrm{s,p})}s_2^{(\parallel,\perp)}s_3+r_{12}^{(\mathrm{s,p})}r_{45}^{(\mathrm{s,p})}s_2^{(\parallel,\perp)}s_3s_4\end{array}\right]} \tag{12}$$

Here t_{ij}, the partial transmission coefficients at the i/j interface for s- and p-polarized light read

$$t_{ij}^{\mathrm{s}}=\frac{2k_i^{\parallel}(\omega)}{k_i^{\parallel}(\omega)+k_j^{\parallel}(\omega)}\,, \tag{13a}$$

$$t_{ij}^{\mathrm{p}}=\frac{2\sqrt{\varepsilon_i^{\parallel}(\omega)}\sqrt{\varepsilon_j^{\parallel}(\omega)}k_i^{\perp}(\omega)}{\varepsilon_i^{\parallel}(\omega)k_j^{\perp}(\omega)+\varepsilon_j^{\parallel}(\omega)k_i^{\perp}(\omega)}\,. \tag{13b}$$

Based on the expressions for reflectance and transmittance, the absorbance (A) of light in a five-layer system can be easily calculated as $A^{(\mathrm{s,p})}=1-R^{(\mathrm{s,p})}-T^{(\mathrm{s,p})}$.

The results obtained within this theoretical framework are discussed in the subsequent sections.

In practice, the NPs are poly-dispersed in size, and so are their lattice spacing or inter-particle separation. This leads to some lattice disorder which is otherwise considered as a perfectly ordered two-dimensional hexagonal array. One may assume that the NP radii and the data for lattice spacing typically follow Gaussian distribution profiles[56], as observed in most experiments. In such scenario the ensemble-averaged optical response spectra can be calculated by averaging the reflectance, transmittance, and absorbance using the estimates for the mean and standard deviation parameters of NP radii and interparticle spacing. Introduction of mild disorder usually smears or spectrally broadens the peaks and slightly shifts their maxima towards red [51,57,58]. In the suggested format, the procedure is straightforward. For instance, in Ref.[59] it has been successfully applied to describe experimental data for a system of hexagonal arrays of NPs (with mild size dispersion and lattice disorder) at a liquid-liquid interface. However, it makes sense to perform such averaging only in the context of particular experimental data, and thus in this article we will not be demonstrating the effects of such averaging. Though the discussion above considers a specific case of hexagonal lattice as example, the method of handling polydispersity as well as disorder effects and the resulting effects on optical response spectrum would be similar for the case with any other lattice orientation.

Smith's group have studied reflectivity of a low-density system of cubic NPs randomly distributed near a metal film separated from it by a dielectric spacer[60]. They observe dips in reflectivity, qualitatively similar to those predicted in our calculations. In our present article, we show the application of the theory with an example of spherical NPs. We particularly focussed on systems with smaller NPs and arrays of much higher densities, in view of promising applications such as electrochemically variable mirror-on-mirror systems[45,47]. For spherical NPs the most interesting effects emerge at high array densities[47]. Our paper provides the guidelines for systematic studies of such systems that are yet to be performed.

Results and Discussion: Effects of Different Parameters on Optical Response Spectra

Based on the above theoretical formulation, we now evaluate the optical response from the mirror-on-mirror system, depicted in Figure 1, over a spectral range of 400–900 nm. We consider gold (Au) NPs arranged in hexagonal array in water (layer 1) coupled to a thin gold film (layer 4), which is separated from the NPs by a dielectric spacer layer (layer 3). The gold film is placed on glass (layer 5). In this article we assume $\varepsilon_1 = \varepsilon_3 = 1.78$, $\varepsilon_5 = 2.25$, set the characteristic dimension of the dipole

layer (layer 2) to $d = 1$ nm [48], and consider layer 2 and layer 4 as gold with permittivity given by Eq. (1). We now systematically explore the effect of other parameters of the system, comparing results of the theory with full-wave numerical solutions of Maxwell's equations generated by COMSOL.

The coupled localized surface plasmon resonance of the NPs in association with the propagating plasmon on the metallic film gives rise to a number of spectacular features in the optical response spectra of this system, which we will highlight and interpret below.

(a) The effect of NP array lattice constant

Figure 2 depicts the influence of lattice constant on optical response of the mirror-on-mirror structure under study. The spectral profiles of reflectance [top row], transmittance [middle row], and absorbance [bottom row] are shown in black (also denoted by circles). Three different lattice constants— $a = 3R$ [left column], $a = 2.5R$ [middle column], and $a = 2.2R$ [right column]—are considered for the hexagonal array of Au NPs, each NP with radius $R = 10$ nm. Thickness of the Au film is taken here as $h_{\mathrm{f}} = 30$ nm and the dielectric spacer layer is considered as thick as $h_{\mathrm{s}} = 1$ nm. The optical response spectra calculated based on theory are shown as dotted curves, whereas those obtained from numerical simulations using COMSOL are shown as solid curves. Effects of plasmonic coupling in this mirror-on-mirror system comprising film-coupled NPs could be better appreciated by comparing these spectra against the two types of reference curves: those obtained in absence of Au NPs (shown in red, denoted by squares) and in absence of Au film (shown in blue, denoted by triangles). Both are shown in each graph for comparison. The closeness of the theoretical and simulated spectra verifies the accuracy of our simplistic five-layer stack model and the effectiveness of the approximations made.

Over the entire spectral range, reflectance from the film-coupled NPs is found to be quenched as compared to the film alone (Figure 2a). At certain spectral region reflectance from film-coupled NPs even shrinks below the level from the NPs alone. Along with such quenching of reflection, there are three prominent features in the reflectance spectrum of the mirror-on-mirror system. They are very sensitive to the changes in interparticle plasmonic coupling that is controlled by the lattice constant. For $a = 3R$ the features in reflectance spectrum seen in Figure 2(a) are as follows: (i) a reflectance peak at ~530 nm, (ii) a dip in reflectance at ~585 nm, and (iii) steep increase in reflectance at wavelengths longer than the dip's wavelength. These traits could be understood by simultaneously analysing the trends of transmittance and absorbance spectra for the same system, shown in Figures 2(b) and 2(c). The quenching of reflection (w.r.t. that from the metallic film without the layer of NPs) at short wavelengths can be attributed to the enhancement in absorption by film-coupled NPs, mainly up to their collective LSPR wavelength. The prominent dip in reflectance can

therefore be associated with this strong LSPR absorbance peak [cf. Figure 2 (c)]. Beyond that peak wavelength absorption rapidly diminishes. At longer wavelength, increase in transmittance through film-coupled NPs (w.r.t. that from the metallic film without NPs) could be held responsible for the quenched reflectance. This effect gets more evident and is better observed at shorter lattice constants of $a = 2.5R$ and $a = 2.2R$ [cf. Figures 2 (d) and 2(g)].

At shorter lattice constants the plasmonic coupling between the film-coupled NPs gets significantly stronger. This makes the reflectance peak—feature 'i' in Figure 2(a)—to get red-shifted, while becoming much wider and stronger [cf. Figures 2(d) and 2(g)], accounting for above 50% reflectance at peak around 620 nm for $a = 2.2R$. *This dramatic increase in reflectance can prove very useful in designing stress-based sensors, which would provide variable reflectivity readings by sensing the changes in lattice spacing.* We also observe a significant change in the reflection dip (feature ii), which gets red-shifted with the reduction in lattice spacing. For $a = 2.5R$ the reflectance at the wavelength of the dip disappears completely, which encourages switching-based applications of such mirror-on-mirror systems. With lattice constant decreasing, the dip gets wider and the reflectance at the dip changes non-monotonically with, *a*, first getting deeper and then rising to some finite value, as seen for $a = 2.2R$. This can be ascribed to the reduction in peak absorbance; indeed, it gets wider besides being red-shifted, due to intense plasmonic coupling at shorter lattice spacing that gives rise to modes of order higher than dipole. Thus there is a noticeable difference between the simulation and dipolar approximation theory in this case. With shorter lattice constants, at long wavelengths there is increase in transmittance [cf. Figures 2(b), 2(e), and 2(h)] as well as in absorbance [cf. Figures 2(f) and 2(i)]. This accounts for reduction in reflectance at long wavelengths and the resulting quenching of reflectance is found to be larger for film-coupled NPs with shorter lattice spacing.

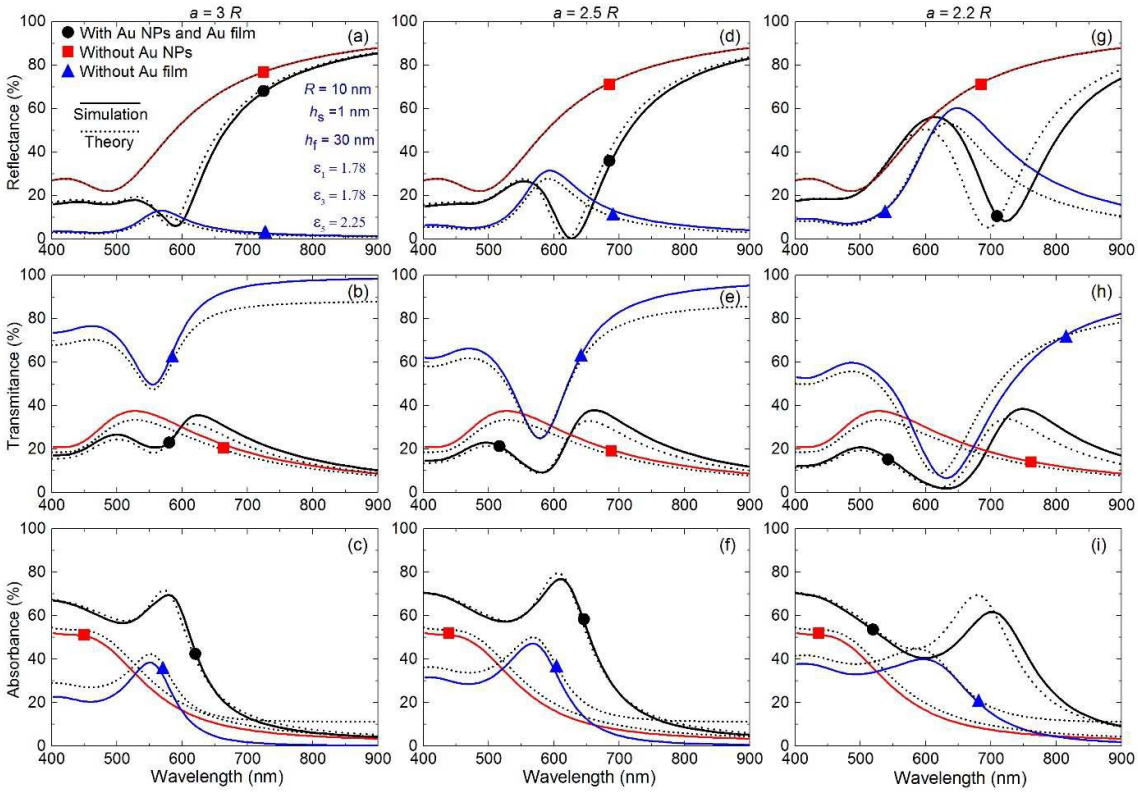

Figure 2. Effect of lattice constant on optical response spectra. Reflectance [top row], transmittance [middle row], and absorbance [bottom row] spectra (shown in black, denoted by circles) of a mirror-on-mirror structure calculated based on theory [dotted curves] as well as using numerical simulations [solid curves] as functions of lattice constant: $a = 3R$ [left column], $a = 2.5R$ [middle column], and $a = 2.2R$ [right column]. Additional 'reference' spectra are included in each subplot: those obtained in absence of gold (Au) nanoparticles (NPs) (shown in red, denoted by squares) and in the presence of NPs but absence of Au film (shown in blue, denoted by triangles). All other system parameters are mentioned in (a).

(b) Effects of spacer layer thickness

Figure 3 depicts the effects of thickness (h_s) of the dielectric spacer layer on the optical response of the mirror-on-mirror system. The legends in this Figure follow the same guidelines used in Figure 2. Here, the lattice constant is fixed at $a = 3R$, but spacer layer thickness is varied as $h_s = 1$ nm, $h_s = 4$ nm, and $h_s = 20$ nm. The thicker the spacer layer that separates Au NPs from the underlying Au film, the weaker is the image-charge interaction. This becomes evident as at

large h_s our theoretical model, based on dipolar approximations only, proves more efficient to match the simulation spectra where contributions from higher order moments are minimal due to weak image interactions [cf. Figures 3(a), 3(d), and 3(g)]; at the same time the studied h_s are not that large that the effects of the finite thickness of the metallic layer, neglected, become important.

Figure 3 shows a monotonic increase in the depth of the reflection dip with increasing h_s. This may be attributed to the monotonous increase in absorption peak with h_s [cf. Figures 3(c), 3(f), and 3(i)]. Moreover the overall reduction of reflection at short wavelengths increases, which is also owing to stronger absorption at larger h_s. This enhancement in absorbance may be attributed to additional absorption by the NPs of light that is reflected from the Au film, which takes place when NP layer is placed at a sufficiently large distance from the film. This would also result in minor reduction in transmittance at short wavelengths [cf. Figures 3(b), 3(e), and 3(h)]. When absorption from film-coupled NPs diminishes at long wavelengths there is no distinguishable difference in transmittance levels at different h_s, resulting in almost identical reflectance in each case, which further supports the above given interpretation.

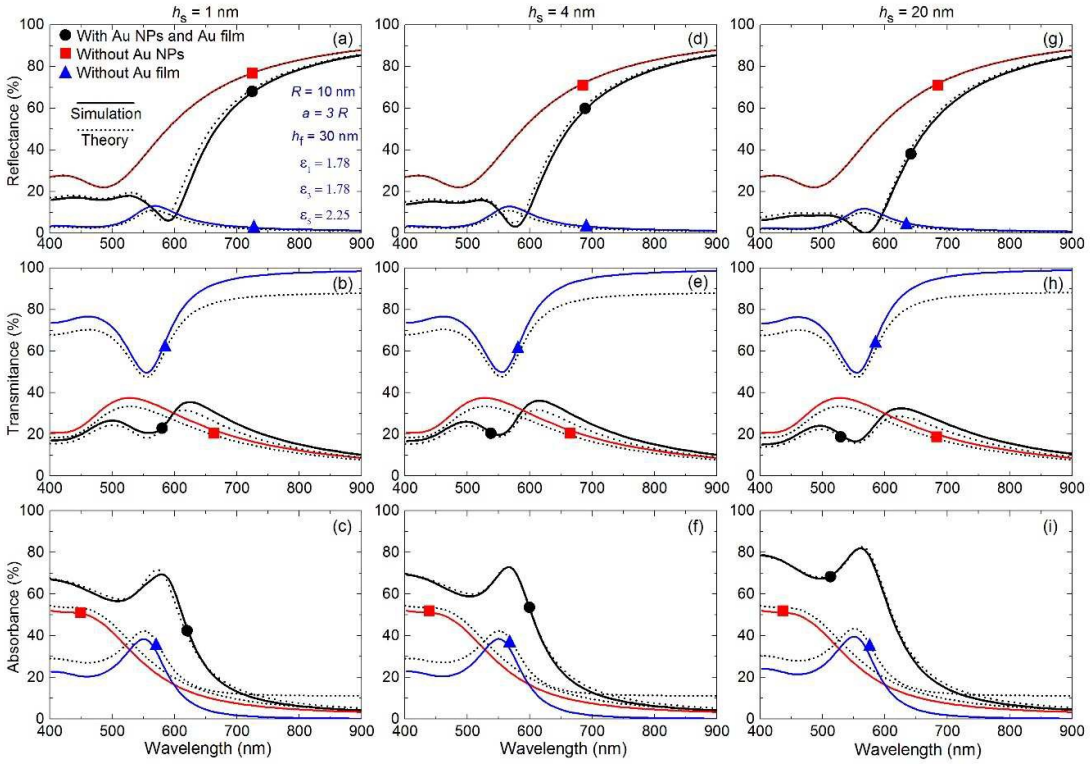

Figure 3. Effects of spacer layer thickness on optical response spectra. Reflectance [top row], transmittance [middle row], and absorbance [bottom row] spectra (shown in black,

denoted by circles) of a mirror-on-mirror structure calculated based on theory [dotted curves] as well as using numerical simulations [solid curves] as function of thickness (or height) of the spacer layer: $h_s = 1$ nm [left column], $h_s = 4$ nm [middle column], and $h_s = 20$ nm [right column]. Additional 'reference' spectra are included in each subplot: those obtained in absence of gold (Au) nanoparticles (NPs) (shown in red, denoted by squares) and in the presence of NPs but absence of Au film (shown in blue, denoted by triangles). All other system parameters are mentioned in (a).

(c) Effects of metallic film thickness

The effects of thickness (h_f) of the metallic film on the optical response spectra of the mirror-on-mirror system are depicted in Figure 4. The legends in this Figure follow the same guidelines used in Figures 2 and 3. Here, the spacer layer thickness is kept constant at $h_s = 1$ nm whereas the thickness of the metallic film is varied as $h_f = 50$ nm, $h_f = 80$ nm, and $h_f = 110$ nm. We discuss only the features from film-coupled NPs where the reference spectra, one without the NPs and another without the film, can be used for comparison and better understanding of plasmonic coupling effects.

As we see from Figure 4, the effects of the variation of metal film thickness on reflection spectra at normal incidence in the studied range of h_f are small, however the trend is interesting. Apart from the long wavelength range (above some 700 nm), the reflection curves tend to go lower and the dip in the reflection spectrum reaches zero reflection with the increase in h_f [c.f. Figures 4(a), 4(d), and 4(g)]. At a first glance it looks surprising, because thicker metal film should suppress transmission [c.f. Figures (4(b), 4(c), and 4 (h)]; why then the reflection gets weaker? But for thicker film we see even stronger enhancement of absorption (both for the reference spectrum without NPs, and with them, [cf. Figures 4(c), 4(f), and 4(i)]. This enhanced absorption causes transmission to get completely diminished over the entire spectral region [cf. Figures 4(b), 4(e), and 4(h)] at large film thickness, but on the other hand it suppresses reflection even stronger: the position of the reflectivity dip coincides with the maximum of absorption.

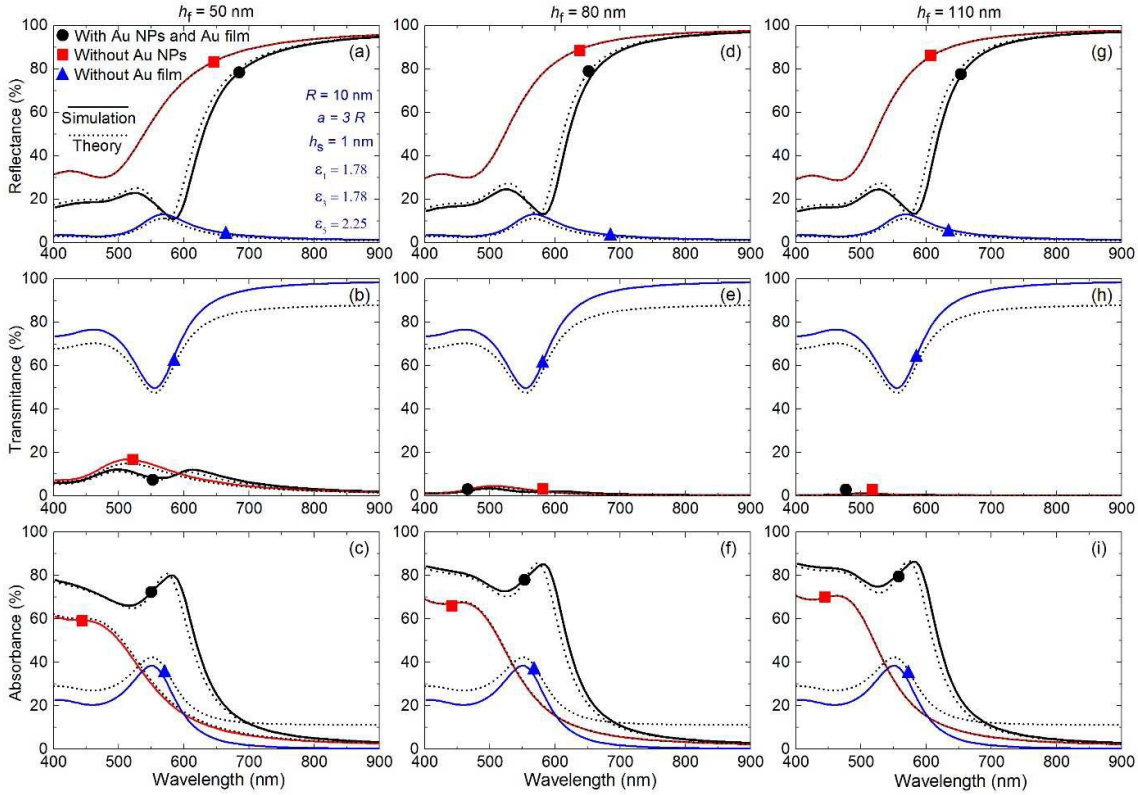

Figure 4. Effects of metallic film thickness on optical response spectra. Reflectance [top row], transmittance [middle row], and absorbance [bottom row] spectra (shown in black, denoted by circles) of a mirror-on-mirror structure calculated based on theory [dotted curves] as well as using numerical simulations [solid curves] as function of thickness (or height) of the metallic film: $h_f = 50$ nm [left column], $h_f = 80$ nm [middle column], and $h_f = 110$ nm [right column]. Additional 'reference' spectra are included in each subplot: those obtained in absence of gold (Au) nanoparticles (NPs) (shown in red, denoted by squares) and in the presence of NPs but absence of Au film (shown in blue, denoted by triangles). All other system parameters are mentioned in (a).

At the same time, at long wavelength, above 700 nm, Figure 4 shows mild increase of reflectance with film thickness. At long wavelengths, it is used to be transmission that would cause quenching of reflection from the metal film; simultaneously the effect of the NP array at long wavelengths vanishes with the increase of wavelength. But as in case of thick metallic film, transmission is negligible, hence there is no quenching effect due to transmission, and the reflectance reaches the level of reflection from the film, or practically from semi-infinite metal alone, because the effect of the NP array at such wavelengths becomes negligible. The highest reflectance

level at long wavelength increases with Au film thickness, but it tends to saturate for $h_f = 110$ and beyond. Additional computations testify this fact and we chose not to explicitly present those spectra here.

(d) Effects of nanoparticle size

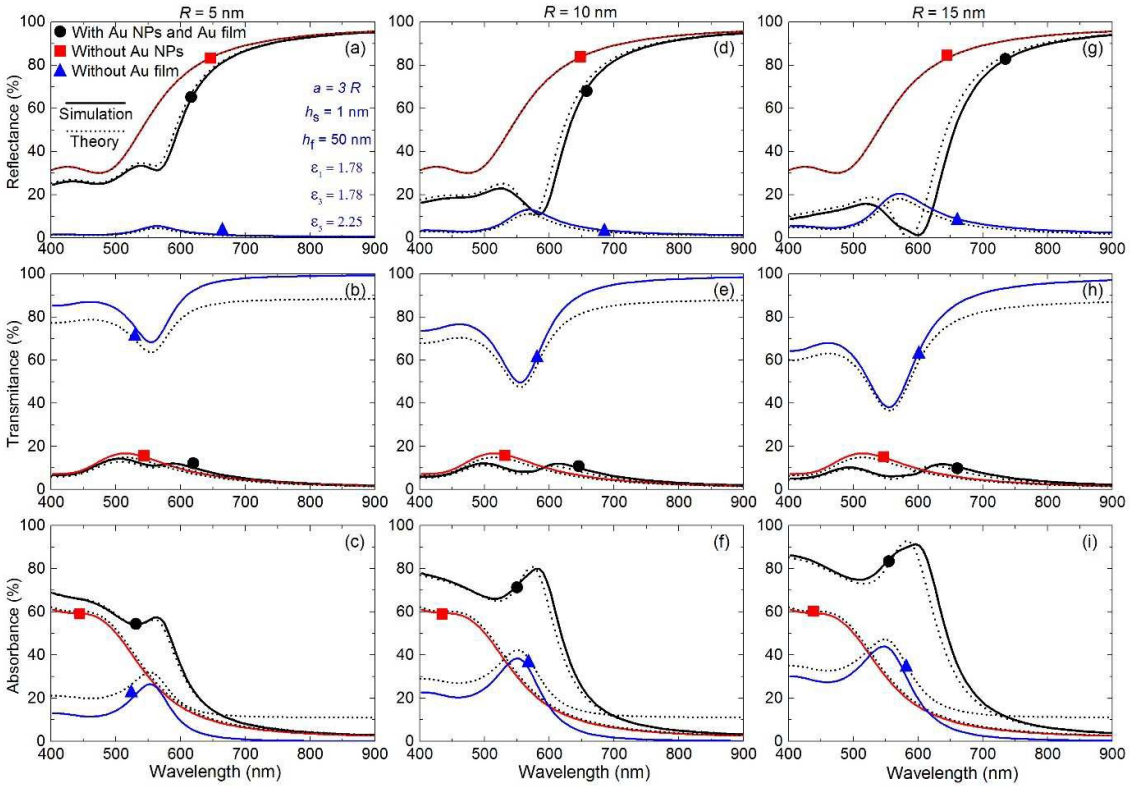

Figure 5. Effects of nanoparticle size on optical response spectra. Reflectance [top row], transmittance [middle row], and absorbance [bottom row] spectra (shown in black, denoted by circles) of a mirror-on-mirror structure calculated based on theory [dotted curves] as well as using numerical simulations [solid curves] as function of nanoparticle radius: $R = 5$ nm [left column], $R = 10$ nm [middle column], and $R = 15$ nm [right column]. Additional 'reference' spectra are included in each subplot: those obtained in absence of gold (Au) nanoparticles (NPs) (shown in red, denoted by squares) and in the presence of NPs but absence of Au film (shown in blue, denoted by triangles). All other system parameters are mentioned in (a).

The influence of NP size on the optical responses of the film-coupled NPs are depicted in Figure 5. The guidelines for the legends in this Figure also remains the same. NP size is varied from $R = 5$ nm to $R = 10$ nm to $R = 15$ nm, at film thickness and all other systems parameters kept constant, except for the array's lattice constant: in this study NP radius is increased while

maintaining a fixed ratio of $a/R = 3$. In other words, the interparticle gap gets adjusted accordingly to the new radius. This allows one to analyse the effect of increase in NP size in combination with linear scaling of the lattice spacing. As expected, the smaller the size of NPs, the better is the match between theory and simulations (as multipolar modes becomes more important at larger sizes). However, in the range of the studied radii the discrepancy is still minor.

The effects of the particle size on optical response spectra are significant. The most profound one is on the dip of the reflectance spectrum of the film-coupled NPs that gets red-shifted, deeper, and wider for larger NPs [cf. Figures 5(a), 5(d), and 5(g)]. This could be directly associated with the monotonic red-shift, strengthening and broadening of the LSPR absorbance peak of the film-coupled NPs [cf. Figures 5(c), 5(f), and 5(i)]. As the film thickness and the lattice spacing are kept constant the transmission characteristics (especially the second peak and its right tail) remain unaltered with change in NP size. However, the transmission peak at shorter wavelength weakens with NP size. At that spectral region absorption of light gets significantly enhanced for large NPs.

Notice that all middle rows of Figures 2–5, show a substantial difference of the transmission from the NP array without the Au film, as calculated by theory and computed by simulation, especially at wavelengths longer than the collective LSPR of the NPs. In such cases, the NPs are assumed to be supported by semi-infinite glass with a spacer layer of height h_s in between (because to 'remove' the metal film we replaced it by the glass). The enhanced transmittance seen in simulation spectra at long wavelengths and for larger lattice sizes could well be due to constructive interference in the far-field between the incident light and the one scattered by the NP layer. As the NPs come closer, the transmission discrepancies seen to reduce [cf. Figures 2(b), 2(e), and 2(h)]. There is no noticeable effect of spacer thickness in enhancing the transmission and the effect of film thickness is irrelevant in this context. However, there is significant effect of the NP size. With increase in NP size for a maintained ratio of lattice constant to NP radius, the transmission at long wavelengths reduces. The difference between theory and simulation in estimating transmission therefore gets smaller for larger NPs [cf. Figures 5(b), 5(e), and 5(h)].

(e) Effects of incidence angle and polarization of the impinging light

Thus far, Figures 2-5 have shown case studies for normal incidence of light, which makes optical responses from the mirror-on-mirror system independent of light polarization, be it reflection, transmission, or absorption. At off-normal incidence of light, optical responses for s- and p-polarized light would be different, cf. Eqs. (9) and (12). In Figures 6 (a)–(c) we demonstrate the

effect of the angle of incidence, for s- and p-polarized light. In each graph, depicted as solid black curves, we show for reference the results of normal incidence for which s- and p-curves coincide. The reflectance spectra for *all angles* shown in Figure 6(a) feature a peak at short wavelength, followed by a dip (causing total zero or almost zero reflection) and then a steep increase in reflectance at long wavelength. The reflection dip corresponds to the LSPR absorption peak shown in Figure 6(c). Interestingly, transmittance in Figure 6(b) exhibits two distinct peaks with stronger transmission at longer wavelengths. How these spectral features evolve as a function of light incidence angle and polarization deserves attention.

One would commonly expect the reflectance to increase with deviation from normal incidence. Indeed, Figure 6(a) shows such trend over the entire spectral region for s-polarized light, with significant enhancement at large incident angle. But with p-polarized light, reflectance undergoes an opposite trend at small incident angle (e.g., $\theta = 30^\circ$); at larger angle $\theta = 60^\circ$ this effect is noticeable only at short and at long wavelengths. At nonzero incident angle, the dip in reflectance experiences red and blue shifts for s- and p-polarized light, respectively. The depth of the reflectance minimum gets smaller with the angle of incidence, for s-polarized light, but it practically does not change for p-polarization.

The effect on transmission spectrum is rather monotonous, as shown in Figure 6(b). For both s- and p-polarized light at any nonzero incidence angle, transmission reduces over the entire spectrum, apart from the long wavelengths range where p-polarized light shows marginal increase in transmission. Transmission of s-polarized light is found to be comparatively lesser than p-polarized light, and this difference in transmittance increases with θ .

The trends in absorbance as a function of light incident angle and polarization are shown in Figure 6(c). Absorbance at short wavelengths can be associated with the LSPR absorbance peak, which is found to get blue-shifted and stronger (red-shifted and weaker) at larger incident angle for p-polarized (s-polarized) light, respectively. These trends can be directly associated with the shift in reflectance dip characteristics as seen in Figure 6(a). The stronger the absorbance peak, the deeper is the reflectance dip. Besides the depth of reflectance minimum, its spectral position can also be tuned by altering incident light characteristics. This finding is vital in designing futuristic optical devices with dynamically tuneable switching abilities at different wavelengths.

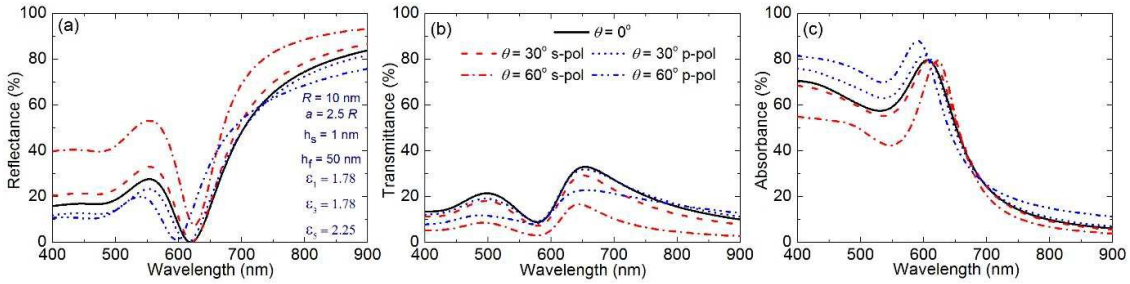

Figure 6. Effects of incident angle and polarization of light on optical response spectra. Theoretically calculated optical spectra depicting reflectance (a), transmittance (b), and absorbance (c) at different incident angle θ for s- and p-polarized light. All other system parameters are mentioned in (a).

(f) Summary of the main trends to be exploited in tuneable mirror-on-mirror platforms

- When lattice constant gets shorter which brings the NPs closer, the high-energy reflectance peak grows besides getting red-shifted and broader. The reflection dip also follows similar trends while getting deeper, and its spectral position strictly follows the absorption peak. The single peak seen in the absorption spectrum gets red-shifted and broadened, but peak absorbance got weaker at very short lattice spacing where there is finite reflectance at the dip wavelength. The high-energy transmission peak weakens. At short lattice constants the low-energy transmission peak is found to be more sensitive to enhancement in plasmonic coupling as it gets significantly red-shifted, stronger and broader.

- The reflection dip is found to be tuneable by changing the thickness of the dielectric spacer layer, where the dip gets blue-shifted and features lower minimum for a thicker spacer. With increase in metallic film thickness there is no prominent changes in the reflectance profile, however, the reflection dip gets slightly shallower. Transmission drops dramatically over the entire spectral region as light gets strongly absorbed by a thicker film.

- For larger NPs, there is more quenching of the reflection over the entire spectrum. Reflection dip gets wider, deeper, and red-shifted. Low energy transmission peak gets largely red-shifted, however overall transmission reduces. Significant increase in absorption is witnessed with its peak getting stronger as well as broader.

- Transmittance reduces for both s- and p-polarized light with the increase of the incident angle; more reduction is seen in the case of s-polarization. Notably, the reflection increases with theta for s-polarized light whereas decreases for p-polarization. At larger incident angle

this difference in reflection gets larger. The position and the depth of the reflection minimum can be tailored as functions of light incident angle and polarization. The trend in the reflection dip is dictated by a reverse trend seen in the absorption peak.

Conclusions

We developed a comprehensive framework—based on combined theories of quasi-static dipolar approximations, image-charge interactions, and multi-layer reflection—that appears to be accurate in describing optical response spectra of mirror-on-mirror structures. Explicit expressions are derived to estimate optical responses—reflectance, transmittance, and absorbance spectra—of a hexagonal array of gold nanospheres coupled to a gold film of finite thickness. The nanospheres immersed in water or another dielectric medium are considered to assemble forming a hexagonal array on top of a dielectric spacer that separates the NP layer from an underlying gold film, which is placed on a semi-infinite glass slab.

We investigated the optical response spectra of such a mirror-on-mirror system over the spectral range of 400 nm to 900 nm, identified many exciting new features and analysed those as functions of the lattice constant, thickness of spacer layer and gold film, NP size, and characteristics of incident light. The accuracy of the predictions of the model are compared against those obtained from full-wave numerical simulations. In general, the model is found to be very accurate and efficient within the scope of quasi-static approximation. However, its accuracy degrades for dense arrays of large nanoparticles (radii>25 nm, and/or interparticle distances<2.2a)) and when placed very close to the metallic film, where quasi-static approximations are not adequate.

The reflection from the mirror-on-mirror system under study is found to undergo quenching as compared to that from the film in absence of NPs. The underlying physical reason being the interplay of contributions from absorption and transmission by the film-coupled NPs as function of wavelength and various system parameters. The reflectance spectrum bears the features of a peak at short wavelength, followed by a dip beyond which reflectance level steeply rises that tends to match the reflectance from the film alone at long wavelengths. Transmission spectrum of the film-coupled NPs features two distinct peaks, whereas there is only one dominant peak in absorption that steeply diminishes at long wavelengths.

As summarized in the previous section, the reflection dip can be tuned by changing the size of NPs, distance between them and thickness of the dielectric spacer.

System parameters such as the position of the layer of NPs relative to the interface and the average distance between NPs can be controlled by various means. At electrode/electrolyte interfaces this could be achieved through the variation of electrode potential. The latter will affect the coverage of the interface by NPs or their position relative to the interface if NPs are anchored to the interface by spacer ligands. Indeed, polarizing electrode negatively, negative NPs will be less favoured to adsorb at the interface or be stimulated to fully desorb from it, if they are not anchored. Other factors that can control the structure of mirror-on-mirror platform are: the population of NP concentration of electrolyte in the liquid phase, charge of the functional groups (depending on their nature often controllable by the solution pH), and the length of the anchoring chains if NPs are anchored (this will affect the maximum separation between the NPs and the metal surface).

The theory used here will be helpful in customizing an otherwise challenging system to realize configurations of interest. After the experimental verification of the discussed predictions, a systematic scan over geometrical parameters might reveal configurations that maximize reflection (configurable mirror), absorption (perfect absorber) and transmission (extraordinary transmission through metallic film), one at a time. Such a study would be practically impossible based on just full-wave solvers.

This work thus provides a platform for designing and optimizing tuneable mirror-on-mirror systems to act as smart optical metamaterials. Independently, with appropriate choice of materials for different layers in the stacked model, this formalism can be applied in the context of solar energy harvesting, for designing layered NP-assisted solar cells.

Competing interests

The authors declare no competing financial interest.

Authors' contribution

A.A.K., D.S, and M.U. conceived the project; D.S., A.A.K., and MU developed the theory; D.S. carried out all theoretical calculations; D.S. and S.B.H. designed the numerical simulation model; D.S. performed all the simulations, S.B.H. having performed few preliminary once; all authors (D.S., A.A.K., M.U., S.B.H., and J.E.) contributed to analysis of results. D.S. and A.A.K. prepared the first draft of the paper and all authors participated in finalizing it.

Funding

A.A.K. acknowledges the European Science Foundation FP7-MPP-2011 grant "Nanodetector" and the grant of the Engineering and Physical Sciences Research Council UK, "Electrotuneable Molecular Alarm" EP/L02098X/1. S.B.H. acknowledges support of "Stichting voor Fundamenteel Onderzoek der Materie" (FOM) for the program "Stirring of light!", which is part of the "Nederlandse Organisatie voor Wetenschappelijk Onderzoek" (NWO).

Acknowledgement

The authors are thankful for discussions of various aspects of this emerging area with Y. Montelongo and L. Velleman from Imperial College London.

References

1 U. Kreibig and M. Vollmer, *Optical Properties of Metal Clusters*, Springer-Verlag, Berlin, 1995.

2 P. Guo, D. Sikdar, X. Huang, K. J. Si, W. Xiong, S. Gong, L. W. Yap, M. Premaratne and W. Cheng, *Nanoscale*, 2015, **7**, 2862–8.

3 S. Lal, S. Link and N. J. Halas, *Nat. Photonics*, 2007, **1**, 641–648.

4 S. A. Maier, *Plasmonics: Fundamentals and Applications*, Springer, 2007.

5 W. Xiong, D. Sikdar, M. Walsh, K. J. Si, Y. Tang, Y. Chen, R. Mazid, M. Weyland, I. D. Rukhlenko, J. Etheridge, M. Premaratne, X. Li and W. Cheng, *Chem. Commun. (Camb).*, 2013, **49**, 9630–2.

6 W. Zhu, D. Sikdar, F. Xiao, M. Kang and M. Premaratne, *Plasmonics*, 2014, 10.1007/s11468–014–9875–0.

7 Q. Shi, K. J. Si, D. Sikdar, L. W. Yap, M. Premaratne and W. Cheng, *ACS Nano*, 2016, acsnano.5b06206.

8 W. L. Barnes, A. Dereux and T. W. Ebbesen, *Nature*, 2003, **424**, 824–830.

9 S. A. Maier, M. L. Brongersma, P. G. Kik, S. Meltzer, A. A. G. Requicha and H. A. Atwater, *Adv. Mater.*, 2001, **13**, 1501–1505.

10 D. Sikdar, I. D. Rukhlenko, W. Cheng and M. Premaratne, *Plasmonics*, 2014, **9**, 659–672.

11 K. J. Si, D. Sikdar, Y. Chen, F. Eftekhari, Z. Xu, Y. Tang, W. Xiong, P. Guo, S. Zhang, Y. Lu, Q. Bao, W. Zhu, M. Premaratne and W. Cheng, *ACS Nano*, 2014, **8**, 11086–11093.

12 K.-S. Lee and M. A. El-Sayed, *J. Phys. Chem. B*, 2006, **110**, 19220–19225.

13 W. Xiong, D. Sikdar, L. W. Yap, P. Guo, M. Premaratne, X. Li and W. Cheng, *Nano Res.*, 2016, **9**, 415–423.

14 P. Bharadwaj, B. Deutsch and L. Novotny, *Adv. Opt. Photonics*, 2009, **1**, 438–483.

15 D. Sikdar, W. Cheng and M. Premaratne, *J. Appl. Phys.*, 2015, **117**.

16 P. K. Jain, K. S. Lee, I. H. El-Sayed and M. A. El-Sayed, *J. Phys. Chem. B*, 2006, **110**, 7238–7248.

17 C. Noguez, *J. Phys. Chem. C*, 2007, **111**, 3806–3819.

18 K. L. Kelly, E. Coronado, L. L. Zhao and G. C. Schatz, *J. Phys. Chem. B*, 2003, **107**, 668–677.

19 A. B. Evlyukhin, C. Reinhardt, A. Seidel, B. S. Lukyanchuk and B. N. Chichkov, *Phys. Rev. B*, 2010, **82**, 45404.

20 F. Le, D. W. Brandl, Y. A. Urzhumov, H. Wang, J. Kundu, N. J. Halas, J. Aizpurua and P. Nordlander, *ACS Nano*, 2008, **2**, 707–718.

21 K. J. Si, D. Sikdar, L. W. Yap, J. K. K. Foo, P. Guo, Q. Shi, M. Premaratne and W. Cheng, *Adv. Opt. Mater.*, 2015.

22 P. Guo, D. Sikdar, X. Huang, K. J. Si, B. Su, Y. Chen, W. Xiong, L. Wei Yap, M. Premaratne and W. Cheng, *J. Phys. Chem. C*, 2014, **118**, 26816–26824.

23 Y. Chen, K. J. Si, D. Sikdar, Y. Tang, M. Premaratne and W. Cheng, *Adv. Opt. Mater.*, 2015, **3**, 919–924.

24 Y.-F. Chau and Z.-H. Jiang, *Plasmonics*, 2011, **6**, 581–589.

25 J. Hu, W. Cai, H. Zeng, C. Li and F. Sun, *J. Phys. Condens. Matter*, 2006, **18**, 5415.

26 T. Hutter, S. R. Elliott and S. Mahajan, *Nanotechnology*, 2013, **24**, 35201.

27 M. W. Knight, Y. Wu, J. B. Lassiter, P. Nordlander and N. J. Halas, *Nano Lett.*, 2009, **9**, 2188–2192.

28 J. Y. Ou, E. Plum, L. Jiang and N. I. Zheludev, *Nano Lett.*, 2011, **11**, 2142–2144.

29 N. I. Zheludev and Y. S. Kivshar, *Nat. Mater.*, 2012, **11**, 917–924.

30 B. Luk'yanchuk, N. I. Zheludev, S. A. Maier, N. J. Halas, P. Nordlander, H. Giessen and C. T. Chong, *Nat. Mater.*, 2010, **9**, 707–715.

31 Z. Huang, A. Baron, S. Larouche, C. Argyropoulos and D. R. Smith, *Opt. Lett.*, 2015, **40**, 5638.

32 C. Ciracì, X. Chen, J. J. Mock, F. McGuire, X. Liu, S.-H. Oh and D. R. Smith, *Appl. Phys. Lett.*, 2014, **104**, 023109.

33 J. J. Mock, R. T. Hill, Y.-J. Tsai, A. Chilkoti and D. R. Smith, *Nano Lett.*, 2012, **12**, 1757–1764.

34 J. J. Mock, R. T. Hill, A. Degiron, S. Zauscher, A. Chilkoti and D. R. Smith, *Nano Lett.*, 2008, **8**, 2245–2252.

35 J. J. Mock, R. T. Hill, Y.-J. Tsai, A. Chilkoti and D. R. Smith, *Nano Lett.*, 2012, **12**, 1757–1764.

36 V.-V. Truong and B. de Dormale, *Plasmonics*, 2011, **6**, 195–200.

37 C. Ciracì, X. Chen, J. J. Mock, F. McGuire, X. Liu, S.-H. Oh and D. R. Smith, *Appl. Phys. Lett.*, 2014, **104**, 023109.

38 J. J. Mock, R. T. Hill, A. Degiron, S. Zauscher, A. Chilkoti and D. R. Smith, *Nano Lett.*, 2008, **8**, 2245–2252.

39 A. Aubry, D. Y. Lei, A. I. Fernández-Domínguez, Y. Sonnefraud, S. A. Maier and J. B. Pendry, *Nano Lett.*, 2010, **10**, 2574–2579.

40 H. A. Atwater and A. Polman, *Nat. Mater.*, 2010, **9**, 205–213.

41 Z. Huang, A. Baron, S. Larouche, C. Argyropoulos and D. R. Smith, *Opt. Lett.*, 2015, **40**, 5638.

42 E. A. Smirnov, P. Peljo, M. Scanlon, F. Gumy and H. Girault, *Nanoscale*, 2016.

43 R. T. Hill, K. M. Kozek, A. Hucknall, D. R. Smith and A. Chilkoti, *ACS Photonics*, 2014, **1**, 974–984.

44 M. K. Bera, H. Chan, D. F. Moyano, H. Yu, S. Tatur, D. Amoanu, W. Bu, V. M. Rotello, M. Meron, P. Král, B. Lin and M. L. Schlossman, *Nano Lett.*, 2014, **14**, 6816–6822.

45 J. B. Edel, A. A. Kornyshev and M. Urbakh, *ACS Nano*, 2013, **7**, 9526–9532.

46 J. Paget, V. Walpole, M. Blancafort Jorquera, J. B. Edel, M. Urbakh, A. A. Kornyshev and A. Demetriadou, *J. Phys. Chem. C*, 2014, **118**, 23264–23273.

47 J. B. Edel, A. A. Kornyshev, A. R. Kucernak and M. Urbakh, *Chem. Soc. Rev.*, 2016, **45**, 1581–1596.

48 A. A. Kornyshev, M. Marinescu, J. Paget and M. Urbakh, *Phys. Chem. Chem. Phys.*, 2012, **14**, 1850.

49 M. E. Flatté, A. A. Kornyshev and M. Urbakh, *J. Phys. Chem. C*, 2010, **114**, 1735–1747.

50 V.-V. Truong and B. de Dormale, *Plasmonics*, 2011, **6**, 195–200.

51 B. N. J. Persson and A. Liebsch, *Phys. Rev. B*, 1983, **28**, 4247–4254.

52 A. Bagchi, R. G. Barrera and R. Fuchs, *Phys. Rev. B*, 1982, **25**, 7086–7096.

53 M. Born and E. Wolf, *Principles of optics: Electromagnetic theory of propagation, interference and diffraction of light*, Cambridge University Press, 1999.

54 D. Sikdar, I. D. Rukhlenko, W. Cheng and M. Premaratne, *J. Opt. Soc. Am. B*, 2013, **30**, 2066–2074.

55 P. B. Johnson and R. W. Christy, *Phys. Rev. B*, 1972, **6**, 4370–4379.

56 J. C. Hulteen, D. A. Treichel, M. T. Smith, M. L. Duval, T. R. Jensen and R. P. Van Duyne, *J. Phys. Chem. B*, 1999, **103**, 3854–3863.

57 T. J. Antosiewicz and T. Tarkowski, *ACS Photonics*, 2015, **2**, 1732–1738.

58 L. Zhao, K. L. Kelly and G. C. Schatz, *J. Phys. Chem. B*, 2003, **107**, 7343–7350.

59. L. Velleman, D. Sikdar, V. Turek, S. Roser, A. A. Kornyshev and J. Edel, ACS Photonics, 2016, Submitted.

60 A. Moreau, C. Ciracì, J. J. Mock, R. T. Hill, Q. Wang, B. J. Wiley, A. Chilkoti and D. R. Smith, *Nature*, 2012, **492**, 86–89.